

# Reports

## Atmosphere of Mars: Mariner IV Models Compared

**Abstract.** *Three classes of models for the atmosphere of Mars differ in identifying the main ionospheric layer measured by Mariner IV as being analogous to a terrestrial F<sub>2</sub>, F<sub>1</sub>, or E layer. At an altitude of several hundred kilometers, the relative atmospheric mass densities for these models (in the order named) are approximately 1, 10<sup>2</sup>, and 10<sup>4</sup>, and the temperatures are roughly 100°, 200°, and 400°K. Theory and observation are in best agreement for an F<sub>2</sub> model, for which photodissociation of CO<sub>2</sub> and diffusive separation result in an atomic-oxygen upper atmosphere, with O<sup>+</sup> being the principal ion in the isothermal topside of the ionosphere. The mesopause temperature minimum would be at or below the freezing point of CO<sub>2</sub>, and dry ice particles would be expected to form. However, an F<sub>1</sub> model, with molecular ions in a mixed and warmer upper atmosphere, might result if photodissociation and diffusive separation are markedly less than would be expected from analogy with Earth's upper atmosphere. The E model proposed by Chamberlain and McElroy appears very unlikely; it is not compatible with the measured ionization profile unless rather unlikely assumptions are made about the values, and changes with height, of the effective recombination coefficient and the average ion mass. Moreover our theoretical heat-budget computations for the atmospheric region probed by Mariner IV indicate markedly lower temperatures and temperature gradients than were obtained for the E model.*

The evidence of Mariner IV (1) has led to three markedly different types of models for the Martian atmosphere. They differ in particular in explaining the characteristics of the main ionization layer observed in the atmosphere over Electris, near 50°S, 177°E, at 1300 hours local time in late winter. By analogy with the formation of ionization layers in Earth's upper atmosphere, we designate the three classes of models F<sub>2</sub>, F<sub>1</sub>, and E.

The F<sub>2</sub> or Bradbury models rest on the assumption that the observed ionization peak results from a rapid upward decrease of the ion-recombination loss coefficient, together with downward diffusion of plasma. In the F<sub>2</sub> models, the electron-density peak is above the region where most of the electron production and recombination occurs.

The F<sub>1</sub> and E models are based on the assumption that the observed ionization profile is a Chapman layer in which the peak coincides with the electron-production peak caused by solar ultraviolet and x-rays, respectively.

Interpretation of the Mariner data in terms of F<sub>2</sub> and F<sub>1</sub> models (Figs. 1 and 2) was first suggested by the radio occultation team (2, 3) and later

expanded (4); the F<sub>2</sub> explanation was favored. A different F<sub>2</sub> model has been proposed (5) and other F<sub>1</sub> models have been discussed (6, 7). Chamberlain and McElroy (8) have offered an E model (Figs. 1 and 2). While rather particular F<sub>2</sub>, F<sub>1</sub>, and E models are shown in Figs. 1 and 2 and are discussed below, most of the arguments that are presented are applicable to a general comparison of these three classes.

Below about 30-km altitude, there is not much latitude in determining the neutral number density and temperature profiles from the measured refractivity, since the atmosphere must consist almost entirely of CO<sub>2</sub> (1). At ionospheric heights, interpretation of the radio occultation data appears to be considerably more ambiguous, with proposed neutral number densities differing by factors up to 10<sup>4</sup> and with suggested upper-atmospheric temperatures varying from about 100° to more than 400°K.

The full drawn curves of Figs. 1 and 2 apply to the F<sub>2</sub> model (2-4). In this model, CO<sub>2</sub> is dissociated into O and CO at about 70-km altitude. Atomic oxygen predominates in the upper atmosphere, if one assumes diffusive equilibrium above the dissociation re-

gion. At the ionization peak (120-km altitude), the atomic-oxygen density was determined by equating the photoionization rate and the rate of downward diffusion of plasma. The CO<sub>2</sub> density at this altitude was estimated by equating the rates of diffusion and recombination loss of electrons. The limiting recombination-loss mechanism at the ionization peak used for this model is  $O^+ + CO_2 \rightarrow O_2^+ + CO$ , with a rate coefficient of  $10^{-9}$  cm<sup>3</sup>/sec (3, 4, 9).

Above the ionization peak the atmospheric temperature for the F<sub>2</sub> model was determined from the observed plasma scale height on the assumption of thermal equilibrium between the plasma components and the neutral gas (2-5). A temperature of about 100°K is obtained by use of a plasma scale height of 29 km (see Fig. 3), which we believe to be more accurate than the values of 20 to 25 km given in the preliminary report (1). Note also (Fig. 3) that the topside scale height does not change noticeably with height, in agreement with the isothermal prediction for an F<sub>2</sub> model.

Between approximately 30- and 100-km altitude above Electris, refractivity was too low to be detected. However, one can utilize the temperature and density of CO<sub>2</sub> above and below to determine the average temperature for this intermediate region (4). On the basis of the theoretical heat-balance computations discussed below, we put the mesopause temperature minimum at an altitude corresponding to a density of about  $10^{13}$  cm<sup>-3</sup>.

The F<sub>2</sub> temperature profile (Fig. 2) dips below the saturation temperature for CO<sub>2</sub> vapor. It is well known that supersaturation of water vapor and supercooling of H<sub>2</sub>O droplets take place in our own atmosphere, and an analogous situation with regard to the gas phase of CO<sub>2</sub> may exist on Mars. If, on the other hand, the sublimation time were shorter than the diffusion time in this region of the atmosphere, one would anticipate the formation of CO<sub>2</sub> particles (4), so that the temperature profile might follow approximately the saturation temperature for CO<sub>2</sub> vapor. This effect might help to explain some of the haze and particle layers observed with Earth-based telescopes and with the Mariner-IV TV camera, and perhaps the high-pressure estimates that were obtained on the basis of optical scattering from the atmosphere of Mars.

The low temperatures required for

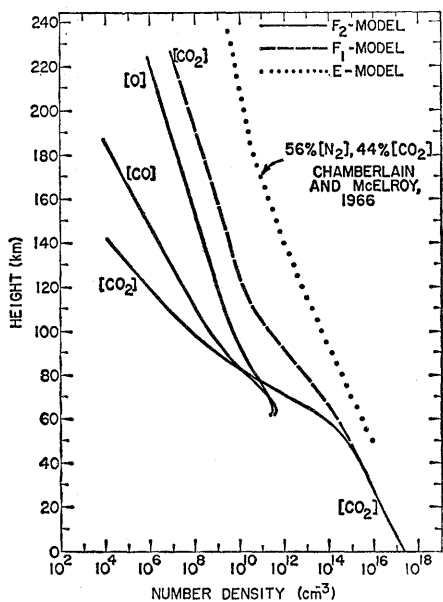


Fig. 1. Number density versus altitude for three different atmospheric models. The  $F_2$  and  $F_1$  models apply to the location and time of immersion into occultation (10); the E model is from (8).

the  $F_2$  model of Figs. 1 and 2, in the atmospheric region between 30- and 100-km altitude, follow from the theory already outlined (4). Other considerations also suggest a cold intermediate region in the Martian atmosphere: for example, radiative-transfer computations for the lower atmosphere have yielded stratospheric temperatures below the saturation temperature for  $CO_2$  vapor (11). Similarly, earlier heat-balance calculations for the upper at-

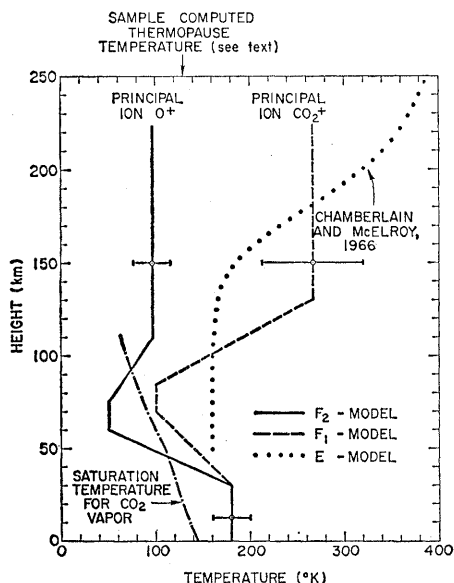


Fig. 2. Temperature versus altitude for three different atmospheric models. The  $F_2$  and  $F_1$  models apply to the location and time of immersion into occultation; the E model is from (8).

mosphere gave a mesopause temperature of  $76^\circ K$  (12).

Chamberlain and McElroy (8) have objected to interpretation of the observed ionization peak as an  $F_2$  region on the grounds that their theoretical estimates yield a thermopause temperature at least four times that of the  $F_2$  model. (On the other hand, see the results and discussion below of other temperature computations.) Instead they suggest that the ionization peak should be interpreted as an E region produced by solar x-rays. The number density and temperature profiles for their model are shown by the dotted curves in Figs. 1 and 2.

In order to interpret the ionization peak as an E layer, one must explain why neither an  $F_1$  nor an  $F_2$  layer was detected, and also how the plasma scale height could remain constant from the E region up to the top of the ionosphere (see Fig. 3).

To avoid formation of an  $F_2$  ionization peak, Chamberlain and McElroy assume that the upper atmosphere is mixed and that  $CO_2^+$  is the predominant ion in the upper regions of the observed layer. For comparison, one may note that Earth's atmosphere is mixed only up to a density of about  $10^{12}$  to  $10^{13} \text{ cm}^{-3}$ , which occurs well below the  $F_2$  and  $F_1$  regions.

The absence of an  $F_1$  ionization peak at about 200-km altitude from Chamberlain and McElroy's model requires the effective recombination coefficient to be greater at this altitude than in the E region below; in Earth's atmosphere it decreases with altitude. In their Martian  $F_1$  region the electron production rate and electron number density are the order of  $10^3 \text{ cm}^{-3} \text{ sec}^{-1}$  and  $10^4 \text{ cm}^{-3}$ , respectively. Thus an effective recombination coefficient of about  $10^{-5} \text{ cm}^3/\text{sec}$  would be necessary in order to account for the low electron density at this altitude. While highly reliable measurements for the dissociative recombination of  $CO_2^+$  apparently are not available, we should point out that this value is two to three orders of magnitude greater than the central values given by Nawrocki and Papa (13) for this process, and is three to four orders of magnitude greater than the effective recombination coefficient at corresponding density levels in Earth's atmosphere.

However, our major objection to an E-region hypothesis is that it is difficult to make compatible with the constant plasma scale height observed above the ionization peak. The measured two-

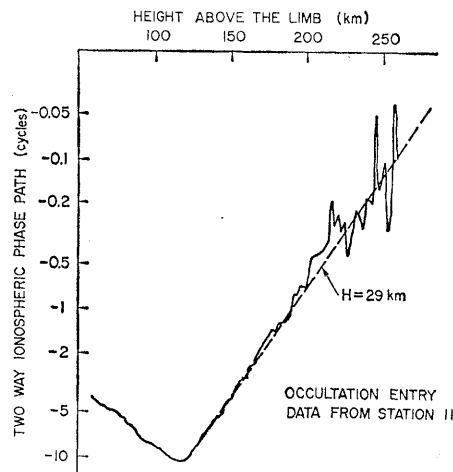


Fig. 3. Two-way ionospheric phase path versus altitude above the limb. The full-drawn curve represents station 11 data; the stippled curve corresponds to a theoretical model ionosphere with a topside plasma scale height of 29 km.

way phase-path data can be presented in such a way as to compare it with assumed constant scale heights for a spherically symmetrical ionosphere—as in Fig. 3, which shows that the plasma scale height is very nearly constant from just above the peak (120 km) to an altitude of 200 km (perhaps even to 250 km), or over a height range of three or four plasma scale heights. Over this same height range, Chamberlain and McElroy suggest an increase in temperature by a factor of about 2.5. In order to maintain a constant plasma scale height in their model it would be necessary for the average ion mass to increase with altitude. With a constant recombination coefficient within the  $F_1$  region, the ion mass would need to be approximately 49 and 57

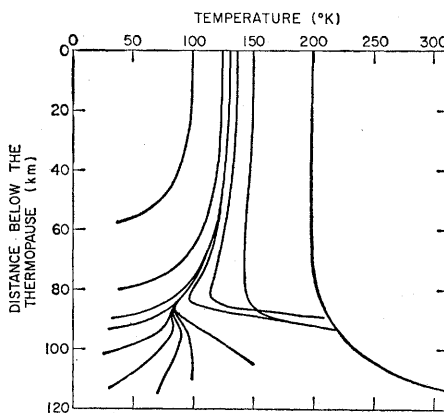


Fig. 4. Temperature versus distance below the thermopause for a sample of theoretical heat-balance calculations discussed in the text. The density at the mesopause, which is the altitude of minimum temperature near the base of the thermosphere, is about  $10^{10} \text{ cm}^{-3}$ .

at 200- and 220-km altitude, respectively, for a plasma scale height of 29 km. [In order to study conditions as high in the ionosphere as possible, we rely principally on data from station 11, since only there could the down-link signal be compared with the same frequency standard as was used to control the up-link signal (*I*). This is the basis for the value given above. However our continuing analyses of data from the other stations agree with Fig. 3 in that the topside scale height does not change significantly with altitude over the range of reliability of the data, and in that its value is somewhat greater than stated in the preliminary report (*I*)—within 20 percent of 29 km.]

If the upper atmosphere of Mars consists primarily of molecular constituents (such as CO<sub>2</sub>, CO, or O<sub>2</sub>), the ionization peak may be located at the density level of maximum electron production by solar ultraviolet flux. This third alternative, denoted as the F<sub>1</sub> model, is also indicated in Figs. 1 and 2 on the assumption of 100 percent CO<sub>2</sub>; in this model the ionization peak occurs at a neutral density of about 10<sup>10</sup> cm<sup>-3</sup>, where the slant optical depth in the ultraviolet part of the spectrum is unity. The topside temperature of this model is about 270°K. Other possible F<sub>1</sub> models based on O<sub>2</sub><sup>+</sup> or CO<sup>+</sup> being the principal ion would have topside temperatures of 195° and 170°K, respectively.

Both the E and F<sub>1</sub> hypotheses that we discuss require mixing or negligible dissociation of CO<sub>2</sub> in order to avoid the preponderance of atomic oxygen in the region where the data show a constant plasma scale height; this is one of the reasons why we favor the F<sub>2</sub> model (3, 4). Comparing only the F<sub>1</sub> and E models, we suggest that the F<sub>1</sub> is more attractive because:

1) No appreciable temperature gradients are expected on the topside of the F<sub>1</sub> layer and the plasma scale height would be constant in this region without us making improbable assumptions about the altitude variations of the ion mass and the recombination coefficient.

2) In the F<sub>1</sub> region of the F<sub>1</sub> model, the recombination coefficient would need to be about 10<sup>-7</sup> cm<sup>3</sup>/sec compared with 10<sup>-5</sup> cm<sup>3</sup>/sec in the F<sub>1</sub> region of the E model. This lower value is in better agreement with the value expected for dissociative recombination of CO<sub>2</sub><sup>+</sup> (13).

In order to understand the physical reasons for the small plasma scale

height and to help resolve ambiguities in interpretation of the occultation data, we have also studied the heat budget of the Martian thermosphere on the basis of similar earlier studies for Earth and the planets (12, 14, 15). Following these studies, we neglect convective and advective transport of heat, together with the effects of temperature transients. The heat balance equation can then be written:

$$\frac{\partial}{\partial h} \left( -\kappa \frac{\partial T}{\partial h} \right) = \sum_i \sum_{\lambda} \epsilon_{\lambda} \sigma_{i\lambda} \frac{1}{2} I_{0\lambda} e^{-\tau_{\lambda}} n_i - \sum_i R_i \quad (1)$$

where *T* is temperature, *h* is altitude, *κ* is thermal conductivity,  $\epsilon_{\lambda}$  is fraction of absorbed solar flux converted to local heat,  $\sigma_{i\lambda}$  is absorption cross section for the *i*th constituent at wavelength  $\lambda$ , *I*<sub>0λ</sub> is solar flux at the top of the atmosphere,  $\tau_{\lambda}$  is

$$\int_h^{\infty} \sum_i \sigma_{i\lambda} n_i \sec \chi \, dh; \text{ optical depth}$$

$\chi$  is solar zenith angle at noon (16), *n<sub>i</sub>* is number density of the *i*th constituent, and *R<sub>i</sub>* is power loss by radiation from the *i*th constituent.

In this equation the divergence of the conducted heat flux is set equal to the input heat power associated with absorption of solar flux, less what is lost through infrared radiation, per unit volume. The factor "1/2" in front of the solar-flux term takes into account, in an approximate way, the fact that the sun only heats the thermosphere about half the time, while the radiative cooling is continuous; the temperatures thus obtained represent approximately a diurnal average profile. In the radiative loss terms (*R<sub>i</sub>*) we have included emission in the CO<sub>2</sub> vibrational bands at 15 μ, the rotational bands at CO, and the 62-μ line of the ground state of O. The effect of the finite atmospheric optical depth in the infrared was also included. The heat-balance calculations outlined here do not apply below the level of vibrational relaxation which, for the F<sub>2</sub> and F<sub>1</sub> models, occurs at approximately 30-km altitude. Below this region the thermal structure is most likely controlled by radiative transfer and convection.

The following technique was used in solving the heat-balance equation with respect to the temperature profile: the atmosphere was divided into stratified layers, and the boundary conditions at the thermopause were chosen

on the basis of the densities and temperatures given in Figs. 1 and 2. Proceeding downward from the thermopause, the temperature and neutral densities were computed in an iterative manner for each layer.

The results of computations based on F<sub>2</sub> number densities, but for different thermopause temperatures, are shown in Fig. 4. (It is not critical at which altitude the thermopause boundary is selected, as long as it is well above the F<sub>1</sub> region where the solar ultraviolet flux is absorbed.) With a boundary condition for the temperature profile of about 100°K at the thermopause, the atmosphere is too cold to conduct the heat flux downward to regions whence it may be radiated. A 200°K temperature at the thermopause is, on the other hand, too high, requiring a great heat flux from below to replace losses by radiation. However, a thermopause temperature of about 130°K gave a reasonable temperature profile for this sample computation. The temperatures in the mesosphere are very sensitive to changes in the boundary conditions at the thermopause. However, the important point to be noted here is not the shape of the profile in the mesosphere (since there are many complex processes affecting temperature in this region), but the fact that these calculations yield a thermopause temperature that is between the approximately 100°K required for the F<sub>2</sub> model and the 270°K required for the F<sub>1</sub> model.

The temperature calculations described here were repeated for several different sets of input parameters (photoabsorption cross sections, solar flux, efficiency of heating, and so on) and boundary densities at the top of the thermosphere. For instance, in some of these calculations the upper atmosphere was assumed to consist of 100-percent CO<sub>2</sub>, corresponding to the F<sub>1</sub> model of Figs. 1 and 2. This assumption gave a higher thermopause temperature than shown in Fig. 4 because the conductivity of CO<sub>2</sub> is lower than for O, and because there is no CO in the F<sub>1</sub> model that can help to radiate the heat away. However, for all of these computations the thermopause temperature over Electris came out between 130 and 280°K; thus, the conclusion remains unchanged (17).

With some convection and perhaps radiation by constituents other than CO<sub>2</sub>, CO, and O, the temperature presumably may be even lower than the 130°K shown in Fig. 4, and thus be

in agreement with the  $F_2$  model. However, if the plasma temperature were higher than the neutral-gas temperature during the measurement, the  $F_1$  model of Figs. 1 and 2 might best agree with these estimates.

Keeping in mind the simplifications used in these temperature studies, and the number of uncertain parameters that enter into the problem, we believe that one cannot reject either the  $F_2$  or the  $F_1$  model on the basis of heat-balance estimates. On this point our work differs markedly from Chamberlain and McElroy's, who claim that the temperature atop the thermosphere must be at least  $400^\circ\text{K}$  (8). There appear to be several reasons for this large disagreement:

1) We made temperature calculations for the thermosphere above Electris; Chamberlain and McElroy, on the other hand, apparently meant their computations to represent a planetary average (18).

2) Radiative cooling is more efficient in the lower thermospheres of our models since they have a higher abundance of  $\text{CO}_2$  (and more  $\text{CO}$  in the case of the  $F_2$  model) than Chamberlain and McElroy's model, which has 56 percent  $\text{N}_2$  and 44 percent  $\text{CO}_2$ . Such a large percentage of  $\text{N}_2$  seems unlikely in view of the small scale height measured near the surface over Electris; it would lead to a temperature that is very nearly the saturation temperature of  $\text{CO}_2$  vapor. So much  $\text{N}_2$  also causes poor agreement between the surface pressures obtained from the occultation measurements and the spectroscopic studies (1, 4).

3) The conductivity for atomic oxygen is between two and three times greater than for a mixture of  $\text{CO}_2$  and  $\text{N}_2$  under equal thermal conditions, and this factor also contributes to the difference in the thermopause temperature for the  $F_2$  and E models of Fig. 2.

4) In the sample calculations shown in Fig. 4, we used lower values for the quiet-sunspot minimum solar flux below  $200 \text{ \AA}$ , based on Johnson's tabulations (19), than those employed by Chamberlain and McElroy.

The temperature calculations that we report show that the small topside-plasma scale height can be explained adequately with either the  $F_2$  or the  $F_1$  model. While our results are quite different from those of Chamberlain and McElroy, they do not preclude an E model with a lower high-latitude thermopause temperature than was used by them. On other grounds, however,

the E-region interpretation appears to be least plausible of the three alternatives.

Smith and Beutler (7) have recently computed a temperature profile for the subsolar region of Mars at sunspot maximum; they assume that  $\text{O}$ ,  $\text{CO}$ , and  $\text{CO}_2$  are in diffusive equilibrium in the upper atmosphere, and obtain a thermopause temperature of approximately  $400^\circ\text{K}$ . While this is the number obtained by Chamberlain and McElroy, there is a large discrepancy because the latter's computations were for sunspot minimum. The results of Smith and Beutler in fact agree well with the sample computations in Fig. 4, since a simple analogy with Earth's upper atmosphere suggests that the thermopause temperatures at sunspot maximum and minimum should differ by more than a factor of two. The remaining difference presumably would be explained by the latitude effect.

Smith and Beutler also attempt to explain the small plasma scale height observed by Mariner IV; they suggest that the observed ionization peak is an  $F_1$ -type layer consisting predominantly of  $\text{O}_2^+$  and with a temperature of  $170^\circ\text{K}$  corresponding to a 25-km plasma scale height. However, this temperature value does not necessarily follow from the theory for such a layer. The  $\text{O}_2^+$  ions in their  $F_1$  region are presumably produced mainly by photoionization of  $\text{O}$ , followed by a charge rearrangement reaction with  $\text{CO}_2$  ( $\text{O}^+ + \text{CO}_2 \rightarrow \text{O}_2^+ + \text{CO}$ ). If so, the plasma scale height should be twice the scale height of the atomic-oxygen profile in the region above the  $F_1$  peak, where ambipolar diffusion is negligible. Thus, in this region, a 25-km plasma scale height would still have to be interpreted in terms of an  $85^\circ\text{K}$  topside temperature. The same is true at greater altitudes, where the lifetime of  $\text{O}^+$  becomes greater than that of  $\text{O}_2^+$ .

Donahue (6) has also suggested that the main ionospheric layer observed on Mars is an  $F_1$  region, with  $\text{O}_2^+$  being the principal ion; however, his atmospheric-temperature profile, which is constant and equal to about  $160^\circ\text{K}$  below 150-km altitude, also appears to be inconsistent with the observed plasma scale height for similar reasons.

Another approach to explanation of the small plasma scale height has been attempted by Gross *et al.* (20); they assume that  $\text{O}^+$  is the principal ion on the topside but introduce temperature gradients in this region in order to

avoid the low temperatures. However, in order to explain the constant scale height, this approach requires a temperature gradient that increases exponentially with altitude. Their temperature profiles do not exhibit this property in the altitude range of interest, and additional assumptions (such as a recombination coefficient that increases with altitude) seem necessary in order to explain the observations.

The number densities and temperatures of the  $F_2$  and  $F_1$  models of Figs. 1 and 2 were derived from the immersion data obtained over Electris, a bright area in the southern hemisphere of Mars. Measurements were also made during emersion from occultation, which occurred over Mare Acidalium, near  $60^\circ\text{N}$ ,  $36^\circ\text{W}$ , at about 2340 hours local time in late summer. The emersion data have been analyzed independently by the Jet Propulsion Laboratory and Stanford University members of the occultation experiment team. Our preliminary values for atmospheric pressure, temperature, and temperature-lapse rate near the surface at Mare Acidalium are about 8.5 mb,  $250^\circ\text{K}$ , and  $2.5^\circ\text{K}/\text{km}$ , respectively, on the assumption of 100-percent  $\text{CO}_2$ . The tropopause was located at approximately 17-km altitude. These values, in good agreement with the emersion results of Kliore *et al.* (21), should be compared with 4.9 mb,  $180^\circ\text{K}$ , and zero lapse rate for the atmosphere over Electris ( $50^\circ\text{S}$ ,  $177^\circ\text{E}$ ; 1300 hours local time, late winter) (1). The emersion values are considerably less certain than the immersion results because the spacecraft transmitter changed its frequency and mode of operation in the middle of the emersion measurements (1); this change causes problems in interpretation of the data. Even so, it is difficult to avoid the conclusion that the surface pressure over Mare Acidalium was at least 50-percent greater than over Electris.

Our calculations of the radii of the two occulting features (measured from the Martian center of mass) show that the radius at Electris ( $\sim 3384 \text{ km}$ ) is approximately 4 km greater than the radius at Mare Acidalium. These calculations were based on the "best trajectory" determined by the orbit-determination group of the Jet Propulsion Laboratory, a timing correction supplied by D. L. Cain of J.P.L., and the limb-diffraction effects observed during signal extinction and commencement. The results agree closely with those of Kliore *et al.* (21), who suggest a 5-km

difference, a value of 3384 km at immersion, and possible errors in the radii of  $\pm 3$  km at immersion and  $\pm 4$  km at emersion.

These tentative results lead to several interesting and important implications. The differences in pressure and radius both suggest that the Martian maria may be lowlands; the bright areas, highlands. This question is of interest with regard to future instrument landings on Mars, both from scientific and engineering considerations. However, local terrain features at the occultation points, greater oblateness than a gravitational-equipotential surface, and atmospheric-circulation patterns may also contribute to the observed differences. The low daytime temperature in the lower atmosphere over Electris tends to support the carbon dioxide polar-cap theory which has been vigorously revived (22). On the other hand, the relatively high temperature obtained at 60°N latitude suggests that the residual late-summer polar cap is not likely to be dry ice, since the nighttime atmospheric temperature was some 100°K above the saturation temperature for CO<sub>2</sub> vapor, and the latitude separation was less than 30°. We are led to the preliminary suggestion that the winter polar cap may be predominantly dry ice, while the bottom part of the thicker central region (23), some of which persists through the summer, may be largely water ice.

The nighttime ionosphere over Mare Acidalium apparently had a density lower than about  $5 \times 10^3$  electrons per cubic centimeter (*I*). This upper limit to the electron-number density does not affect any of the models in Figs. 1 and 2, since they all have short-enough time constants (in fact less than 30 minutes at the electron-density peak) to account for a very low nighttime level of ionization.

While theoretical atmospheric models based on analogies with any one of the ionized regions in Earth's upper atmosphere presumably can be tailored to fit the main ionization layer detected on Mars, we favor models of the F<sub>2</sub> type because they seem to account for the observed ionization profile in the most straightforward way. However, we may have overestimated the degree of photodissociation and diffusion separation—estimates which to a large extent are based on analogies with Earth's atmosphere. If so, the ionization peak should be identified as an

F<sub>1</sub> region; that is, a Chapman layer produced by solar ultraviolet flux (2-4). We suggest that model atmospheres based on parallelism between the Martian ionization peak and the terrestrial E (and also D) region(s) should be rejected, since they are inconsistent with the topside plasma scale height unless rather unlikely assumptions are made about the value, and changes with height, of the average ion mass and the recombination coefficient.

Arguments based on simplified temperature computations have been used to question the validity of F<sub>2</sub> models and to support an E model (8). However, thermopause temperatures for the F<sub>2</sub> and F<sub>1</sub> models bracket temperatures derived from our similar computations of the heat budget in the upper atmosphere over Electris, so that neither model apparently can be ruled out on this basis. Furthermore, we suggest that such heat-budget studies are not sufficiently precise to serve as the overriding basis for choice of atmospheric models. This conclusion should not be surprising considering the large uncertainties in the present state of the art as it applies to our own atmosphere, even though experimental and theoretical work has been intensive for many decades.

The atmospheric data yielded by the Mariner IV occultation experiment have apparently resolved several important immediate problems, but have also raised many more-definitive questions. Of prime importance in future occultation measurements is ability to detect lower ionization densities and to study both the neutral and ionized portions of the atmosphere over different topographical areas at different latitudes, times of day, and seasons of the year.

Higher sensitivity for ionospheric measurements is needed to help resolve remaining ambiguities in the model studies and in the first-order density and temperature profiles. Sensitivity could be improved by a dual-frequency experiment (24), which would also enable experimental separation of dispersive plasma effects from the nondispersive refraction of the neutral atmosphere. Repeated measurements at many different locations, times, and seasons are of obvious and critical importance in the atmospheric and ionospheric studies; they would also impact on problems related to global Martian weather, the polar caps, topographic and elevation differences between maria and deserts, and the average oblate

shape of the planet. The requirement for repeated measurements obviously points to a simple radio occultation experiment using a planetary orbiter.

GUNNAR FJELDBO

WENCKE C. FJELDBO

VON R. ESHLEMAN

Center for Radar Astronomy, Stanford University, Stanford, California

#### References and Notes

1. A. J. Kliore, *et al.*, *Science* **149**, 1243 (1965); *et al.*, in *Proc. Caltech J.P.L. Lunar Planetary Conf. Pasadena* (September 1965).
2. D. L. Cain *et al.*, in *Proc. Ionospheric Res. Comm. Avionics Panel, Rome* (Advisory Group for Aerospace Research and Development, NATO, September 1965).
3. G. Fjeldbo, *et al.*, in *Proc. Caltech-J.P.L. Lunar Planetary Conf. Pasadena* (September 1965).
4. G. Fjeldbo, W. C. Fjeldbo, V. R. Eshleman, *J. Geophys. Res.* **71**, 2307 (1966).
5. F. S. Johnson, *Science* **150**, 1445 (1965).
6. T. M. Donahue, *ibid.* **152**, 763 (1966).
7. N. Smith and A. Beutler, "A model Martian atmosphere and ionosphere," *Rpt. 66-3* (Univ. of Michigan Radio Astronomy Observatory, Ann Arbor, March 1966).
8. J. W. Chamberlain and M. B. McElroy, *Science* **152**, 21 (1966).
9. F. S. Fehsenfeld, A. L. Schmeltekopf, E. E. Ferguson, *J. Chem. Phys.* **44**, 3022 (1966).
10. Below the dissociation region of the F<sub>2</sub> model there may be layers of O<sub>2</sub> and O<sub>3</sub> [F. F. Marmo and P. Warwick, "Laboratory and theoretical studies in the vacuum ultraviolet for the investigation of the chemical physics of planetary atmospheres," contract NASw-124 quarterly progress reports (Geophysical Corp. of America, Bedford, Mass., 3 August 1960 and 3 August 1961)]. However, the chemical reaction rates are poorly known and the extent of mixing can only be estimated on the basis of analogies with Earth's atmosphere; thus the actual O<sub>2</sub> and O<sub>3</sub> densities are uncertain. We do not go into further detail on this point since these layers would have little effect on the ionization profile at greater altitudes.
11. G. Ohring, *Icarus* **1**, 328 (1963); similar calculations by C. Prabhakara and J. S. Hogan, Jr. [*J. Atmos. Sci.* **22**, 97 (1965)] gave considerably higher stratospheric temperatures.
12. J. W. Chamberlain, *Astrophys. J.* **136**, 582 (1962).
13. P. J. Nawrocki and R. Papa, *Atmos. Processes* (Prentice-Hall, Englewood Cliffs, N.J., 1963).
14. D. R. Bates, *Proc. Phys. Soc. London* **B64**, 805 (1951); I. Harris and W. Priestler, *J. Geophys. Res.* **67**, 4585 (1962); M. Nicolet, *Planet Space Sci.* **5**, 1 (1961).
15. M. B. McElroy, J. L'Ecuyer, J. W. Chamberlain, *Astrophys. J.* **141**, 1523 (1965).
16. The solar zenith angle enters into Eq. 1, causing the thermopause temperature to decrease with increasing solar latitude. This effect is not obvious in Earth's thermosphere—one indication that the mathematical model represented by Eq. 1 is oversimplified. We should point out that most of the parameters that enter into the solution of this equation are poorly known, a fact which introduces additional uncertainties.
17. It can be argued that the 24-hour average-temperature profile should be lower than the temperatures obtained by solution of Eq. 1 with  $\chi$  equal to its noon value, 67°, because the average solar zenith angle was about 75° at Electris on the day of the experiment. The temperatures in fact prevailing in the thermosphere at the time of the measurements were, on the other hand, probably somewhat higher than the diurnal average profile, so that temperatures obtained in this manner may still provide the best basis for comparisons. We have also studied the steady-state temperature profiles for  $\chi = 67^\circ$ , which presumably represent upper limits to the temperatures prevailing in the thermosphere during the occultation experiment.

These computations were done by removing the factor "1/2" in front of the solar-flux term of Eq. 1; this change increased the thermopause temperatures by approximately 50 percent.

18. Private communication with Chamberlain and McElroy indicates that their temperature computations were meant to represent a diurnal and latitudinal planetary average. If, rather, the computations were interpreted as only a diurnal average, they would be applicable to a solar latitude of about 38° on Mars. Thus Chamberlain and McElroy used what corresponds to a daytime mean solar zenith angle of 60°, whereas the average solar zenith angle was about 75° at Electricis on the day of the experiment.
19. Below 200 Å we used the quiet-sunspot minimum solar x-ray intensities given in table 4-4 in F. S. Johnson's *Satellite Environment Handbook* (Stanford Univ. Press, ed. 2, 1965) for the sample calculations of Fig. 4. Between 200 and 1000 Å, we used data from H. E. Hinteregger, L. A. Hall, G. Schmedtke, "Solar XUV radiation and neutral particles

distribution in July 1963 thermosphere," Intern. Space Sci. Symp. 5th, Florence, Italy, 1964. For longer wavelengths, we used data from fig. 4-2 of F. S. Johnson's *Satellite Environment Handbook*. Chamberlain and McElroy presumably used the data of Hinteregger *et al.* for all wavelengths.

20. S. H. Gross, W. E. McGovern, S. I. Rasool, *Science* **151**, 1216 (1966).
21. A. J. Kliore, D. L. Cain, G. S. Levy, "Radio occultation measurement of the Martian atmosphere over two regions by the Mariner IV space probe," *Seventh International Space Science Symposium*, Committee on Space Research (COSPAR), Vienna, May 1966.
22. R. B. Leighton and B. C. Murray, *Science* **153**, 136 (1966).
23. G. de Vaucouleurs, *Physics of the Planet Mars* (Faber and Faber, London, 1954), p. 202.
24. G. Fjeldbo, V. R. Eshleman, O. K. Garriott, F. L. Smith, III, *J. Geophys. Res.* **70**, 3701 (1965).
25. Research supported by NASA grants NGR-05-020-065 and NsG-377.

10 June 1966

## Infrared Analysis of Rat Bone: Age Dependency of Amorphous and Crystalline Mineral Fractions

**Abstract.** *Quantitative infrared spectrophotometric analysis of whole femurs from male rats demonstrates that amorphous calcium phosphate is a major component of bone mineral. The amount of amorphous calcium phosphate in whole bone decreases while the crystalline bone apatite increases during early stages of bone formation. Mature rat bone contains constant levels of both amorphous and crystalline calcium phosphate.*

In the past, it was thought that the inorganic portion of bone tissue was composed of submicroscopic calcium phosphate crystals which generally resemble the geological mineral hydroxyapatite, but recent studies indicate that this conceptually simple, one-compartment model of bone mineral is actually an oversimplification of the physical state of the tissue (1). X-ray diffraction studies of bone show that the mineral fraction is composed of two separate phases, amorphous (noncrystalline) calcium phosphate and crystalline apatite (1). This report presents evidence, based on infrared spectrophotometric analysis, for the two-phased nature of bone mineral which indicates that the amorphous and crystalline calcium phosphate fractions of whole rat bone are interrelated. The significance of this finding not only applies to bone structure and metabolism but also affects the interpretation of many observed physical and chemical properties of bone. The net properties of bone mineral must now be considered as variable averages of the individual properties of its two calcium phosphate constituents (2).

The triply degenerate, antisymmetric bending vibration of the orthophosphate ion absorbs infrared radiation at wave

numbers between 500 and 600  $\text{cm}^{-1}$  for both amorphous calcium phosphate and crystalline apatite. Amorphous calcium phosphate gives a broad and symmetrical single absorption band in this region, while the anisotropic local electric field of crystalline apatite partially splits the degeneracy of this absorption band into a well-defined doublet (3). A third band at 630  $\text{cm}^{-1}$ , arising from first order hydroxide ion librational (hindered rotational) motion, is found as a shoulder on this 600  $\text{cm}^{-1}$  phosphate band only in large synthetic hydroxyapatite crystals (3).

Mixtures of amorphous calcium phosphate and crystalline apatite exhibit varying degrees of splitting for the phosphate ion antisymmetric bending mode, depending upon their weight fractions within the mixture (3). We found a straight line correlation between the degree of this infrared splitting and percentage crystallinity (weight fraction of crystalline apatite) in synthetic samples containing these two phases (4). The method used for determining this splitting quantitatively is shown in Fig. 1. A connecting line is constructed between the points of minimum transmission for the two peaks, marking off the area  $A_1$ . A best base line is then drawn from 450  $\text{cm}^{-1}$  to 700  $\text{cm}^{-1}$

at the top of the absorption band, marking off the area  $A_2$ . Since none of the spectra examined in this study contained a hydroxide ion shoulder at 630  $\text{cm}^{-1}$ ,  $A_2$  always represented only phosphate ion absorption. The areas  $A_1$  and  $A_2$  were measured with the aid of a planimeter, affording relative standard deviations of  $\pm 3$  percent. The ratio of  $A_1$  to  $A_2$ , which we call the splitting fraction (SF), measures the amount of splitting for any given sample with a relative standard deviation of  $\pm 4$  percent.

All spectra were recorded on a Beckman IR-12 infrared spectrophotometer under double beam conditions using the instrument's standard mechanical slit program with a frequency drive speed of 40  $\text{cm}^{-1}$  per minute and a strip chart recorder expansion rate of 50  $\text{cm}^{-1}$  per inch (2.5 cm). In each case, total absorption was adjusted so that transmission was between 85 and 90 percent at the base line. Only those spectra that gave a minimum transmission of 45 to 50 percent as measured at the midpoint of the absorption band (base line to constructed line) were used for SF analysis.

As mentioned previously, this method was applied to the determination of percentage crystallinity in well-defined synthetic calcium phosphate samples (4). However, in order to extend the method to bone tissue, a number of pertinent parameters must be taken into account. These are particle size, sample concentration and path length, extraneous compounds, crystal size and stoichiometry, and protein content.

For infrared analysis our samples were mixed with potassium bromide in the following way. All samples were sieved on 250- to 300-mesh screens after they had been ground in a Spex grinder, and the mineral content of each bone sample was predetermined by a measurement of ash weight, so that we could add an original sample weight containing  $2.0 \pm 0.1$  mg of mineral to  $700 \pm 1$  mg of KBr matrix. The sample and matrix were then blended in a Spex grinder and made into pellets, each being pressed under vacuum in a circular die, 22 mm in diameter, under 30 tons ram force in a Limit 30-ton pellet press (approximately 6000 atm). Thus, particle size and sample-matrix homogeneity can be kept constant, and transparent pellets with reproducible mineral concentrations and path lengths can be obtained.

We found no change in SF values